The role of oxidized Gly25, Gly29 and Gly33 residues on the interactions of Aβ_{1-42} with lipid membranes

Hebah Fatafta,[†] Chetan Poojari,[‡,¶] Abdallah Sayyed-Ahmad,[§] Birgit Strodel,[‖,⊥] and Michael C. Owen[*,#]

†*Institute of Biological Information Processing: Structural Biochemistry (IBI-7), Forschungszentrum Jülich, 52425 Jülich, Germany*

‡*Department of Physics, University of Helsinki, P.O. Box 64, FI-00014, Helsinki, Finland*

¶*Theoretical Physics and Center for Biophysics, Saarland University, Campus E2 6, 66123 Saarbrücken, Germany*

§*Department of Physics, Birzeit University, Birzeit, Palestine*

‖*Institute of Biological information Processing: Structural Biochemistry (IBI-7), Forschungszentrum Jülich, 52425 Jülich, Germany*

⊥*Institute of Theoretical and Computational Chemistry, Heinrich Heine University Düsseldorf, 40225, Düsseldorf, Germany*

#*CEITEC – Central European Institute of Technology, Masaryk University, Kamenice 753/5, Brno 625 00, Czech Republic*

E-mail: michaelowen27@gmail.com

Abstract

Oxidative stress is known to play an important role in the pathogenesis of Alzheimer's disease. Moreover, it is becoming increasingly evident that the plasma membrane of

neurons plays a role in modulating the aggregation and toxicity of Alzheimer's amyloid-β peptide, (Aβ). In this study, the combined and interdependent effects of oxidation and membrane interactions on the 42 residues long Aβ isoform are investigated using molecular simulations. Hamiltonian replica exchange molecular dynamics simulations are utilized to elucidate the impact of selected oxidized glycine residues of Aβ42 on the interactions of the peptide with a model membrane comprised of 70% POPC, 25% cholesterol, and 5% of the ganglioside GM1. The main findings are that, independent of the oxidation state, Aβ prefers binding to GM1 over POPC, which is further enhanced by the oxidation of Gly29 and Gly33 and reduced the formation of β-sheet. Our results suggest that the differences observed in Aβ42 conformations and its interaction with a lipid bilayer upon oxidation originate from the position of the oxidized Gly residue with respect to the hydrophobic sequence of Aβ42 involving the Gly29-XXX-Gly33-XXX-Gly37 motif and from specific interactions between the peptide and the terminal sugar groups of GM1.

Keywords

Amyloid-β peptide, Molecular dynamics, Membrane simulations, oxidative stress, GM1, peptide membrane interactions

1 Introduction

Alzheimer's disease (AD) is a neurodegenerative disorder generally affecting persons 65 years and older (*1*). With no cure currently available, and the generally increasing life expectancy in most societies, the number of people affected by this disorder is expected to increase in the coming years. Several mechanisms have been proposed as the pathological cause of AD, including genetics, cholinergic, tau and amyloid hypotheses (*2–6*). Though no hypothesis has been generally accepted, AD brain features substantiate the most widely accepted amyloid

cascade hypothesis (*7*). In particular, the AD brain is characterized by the presence of senile plaques. The main component of these plaques is the amyloid-β peptide, which is produced by the cleavage of the amyloid precursor protein (APP) by β and γ secretases (*8–10*). Aβ ranges from 39 to 43 amino acids in length, however, Aβ42 is predominant in senile plaques and is known to be more toxic than Aβ40 (*11–13*). The primary structure of Aβ42 is shown in Fig. 1. It extends from the unstructured hydrophilic N-terminal region (Asp1 to Lys16) to the hydrophobic C-terminal region (Ala30 to Ala42), and it is linked by central residues (Leu17 to Gly29) that most often forming a turn conformation. The central residues have been shown to play a role in membrane insertion, and sidechain–sidechain interactions through a backbone bend that brings the two β-sheets together (*14–18*). In addition, the AD brain is commonly characterized by an increase in oxidative stress (*19–23*). The generation of excess reactive oxygen species (ROS) or the dysfunction of the anti-oxidant system can cause an increase in the amount of ROS present in normal cells and subsequently leads to the oxidative stress observed in AD (*24*, *25*). The ROS are produced either enzymatically (for example to kill invaders in macrophages) or as a side reaction (like respiratory chain), and generally kept at low level but not totally eliminated due to their function. They are necessary to maintain homeostasis in cell and play important role in signaling. The brain seems to be sensitive to oxidative damage upon oxidative stress due to high dioxygen (the final electron acceptor) consumption in the brain; approximately 20% of the total body consumption (*26*). It is still controversial whether the accumulation of Aβ increases the level of oxidative stress or that the high level of oxidative stress drives Aβ accumulation (*6*). Studies have shown that Aβ is capable of generating free radicals (*27*, *28*) and shows high affinity to bind metals such as Cu^{2+}, Zn^{2+} (*29–31*).

Though the physiological role of Aβ is not well understood, it was found that Aβ-membrane interactions are essential for Aβ to fulfill its physiological functions. These functions include protecting the body from infections, repairing leaks in the blood-brain barrier, promoting recovery from injury, and regulating synaptic function (*32*, *33*).

Understanding the effect of membrane composition on the conformation of Aβ and its interaction with membranes are essential to explain both its physiological function and its role in AD. It was found that the charge of the lipid head group and the structure of the lipid acyl chains determine the transmembrane stability of Aβ42 in zwitterionic POPC and DPPC bilayers, and anionic POPG bilayers in MD study by Poojari et al. (*17*). In another MD study, Poojari et al. found that Aβ42 mutation altered both its interactions with neuronal membranes and its aggregation propensity (*18*). The neuronal membrane plays a key role in modulating Aβ aggregation (*5*, *34*, *35*). It was found that monosialotetrahexosylganglioside (GM1) the most abundant ganglioside in neurons, affects the conformation of Aβ and its neurotoxicity (*36*). Moreover, it has been suggested that the initial attachment of amyloid protein to the plasma membrane is first triggered by binding to gangliosides due to their extracellular location (*37*). Generally, the Aβ-bound GM1 complex has been identified to be present in the AD brain and it has been found that monomeric Aβ has a high affinity for GM1 (*38*, *39*). Furthermore, it was found that the GM1-binding domain of Aβ42 (Aβ(1-16)) can inhibit the amyloid pore formation via binding to GM1 and blocking the first step in the pore formation mechanism (a stepwise mechanism controlled by the dual effect of gangliosides and cholesterol) (*40*). It was also found that Aβ complex formation is enhanced in lipid bilayers enriched by cholesterol content (*41*, *42*).

The role of Aβ in oxidative stress related mechanisms of AD progression is still unclear. It was shown that Met35 of Aβ plays a critical role in this redox process (*43*, *44*). Several studies found that replacing the sulfur atom in Met35 abolished the neurotoxic effect caused by the native peptide (*44*–*47*). The neurotoxic fragment $A\beta_{25-35}$ was observed to lose its neurotoxicity when Met35 was removed (*48*, *49*). It was further hypothesized that the interaction between the proximal residues Gly33 and Met35 in Aβ42 accelerates the generation of free radical induced oxidative stress (*50*, *51*). Moreover, it has been proposed that the hydrophobic C-terminal region is the seed for Aβ aggregation (*52*). This region includes part of the repeated motif GxxxG spanning residues from Gly25 to Gly37 (*53*).

Others have shown that Gly33 of this motif plays a key role in Aβ toxicity (*50*, *54*). It was further reported that modification of Gly33 like mutation not only affects the structure and the hydrophobic surface of the peptide but also affects the neighboring residues and would likely disrupt the interaction between Phe19 and Leu34.

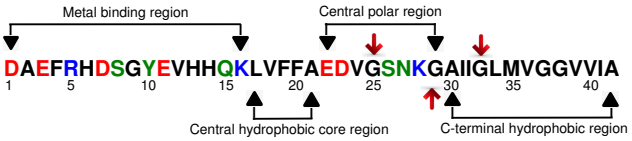

Figure 1: The primary structure of Aβ42, showing the acidic residues in red, the basic residues in blue, the hydrophobic residues in black, and the polar residues in green. The residues forming the metal-binding region, the central hydrophobic core, the central polar region, and the C-terminal hydrophobic region are also indicated. Red arrows point to the oxidized glycine residues investigated in this study.

The relationship between glycine residues in the C-terminal region of Aβ and oxidative stress can be explained by the amyloid radical hypothesis. This hypothesis describes how the C atom of glycine residues is susceptible to the loss of an H-atom upon oxidation of Met35, which in turn causes the formation of a protein backbone radical, stabilized by capto-dative effect (*55*, *56*), that adopts an extended structure perfect for β-sheet formation (*51*). In this hypothesis, Gly33 is predicted to be more susceptible to oxidation by methionine-based sulfuranyl free radical due to the close proximity of these residues in the Aβ42 primary structure. Several experimental studies have been attempted to explore the effect of radicals on proteins but challenges in locating the center of a radical in protein hinders systematic experimental investigations (*57*, *58*).

Studies of Aβ peptide often employ shorter Aβ analogs; however, it is essential to explore the full-length monomeric form of Aβ for a comprehensive understanding of its toxicity (*59*, *60*). Unfortunately, exploring the full-length of Aβ is experimentally challenging due to its high propensity to aggregate. Alternatively, MD simulations can provide insight into the conformational dynamics of Aβ at atomistic resolution, and complements experimental findings (*61*, *62*). Previously, MD simulations have been used to investigate the effect of protein oxidation on protein folding. Owen and coworkers examined the effect of

C_α-centered radical formation on the stability of a model helical peptides in different solvent systems (*63*). Moreover, MD simulations demonstrated the effect of glycine residue radicalization on protein conformation depends both on the protein and the position of the radical (*64*). The effect of radicalization at Gly25 on Aβ42 dimer in solution was further investigated by Liao et. al (*65*). Although the occurrence of oxidative stress in several neurodegenerative diseases is well-established, there is no computational evidence on the effect of radicalization on peptide-membrane interactions.

Thus, in this study we employ both conventional MD simulations, and Hamiltonian replica exchange molecular dynamic (HREMD) simulations to understand the effect of oxidizing glycine residues (25, 29, and 33) on Aβ42 secondary structure and membrane binding. The structure of 1-palmitoyl-2oleyol-phosphatidylcholine (POPC), monosialotetrahexosylganglioside (GM1) and cholesterol (CHOL) used in this membrane are shown in Fig. 2. The parameters of the glycyl radical (GLR) is taken from our previous study (*66*), and the structure of GLR is shown in Fig. S1 in the Supporting Material. HREMD simulations provide an advantage over MD in that it enhances the conformational sampling of the phase space and overcomes the problem of restricting the system to localized low energy regions of the conformational space (*67*).

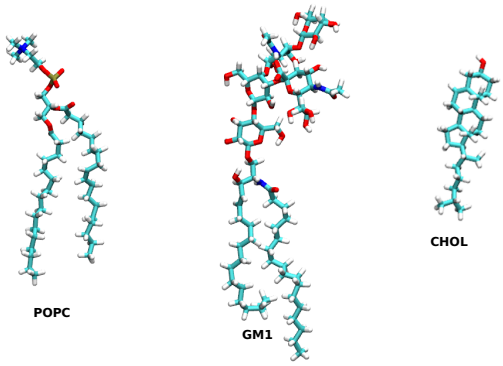

Figure 2: The structure of 1-palmitoyl-2oleyol-phosphatidylcholine (POPC), ganglioside (GM1), and cholesterol (CHOL) used in this work. The structures are shown in licorice representation colored by name, where oxygen atom is shown in red, nitrogen atom is in blue, hydrogen atom is in white and carbon atom in cyan.

2 Results and Discussion

Understanding the neuropathology of Alzheimer's disease (AD) is the driving engine for most research in chemical neuroscience and biology. It is thought that the development of Alzheimer's disease (AD) is related to the interactions between amyloid-β(Aβ) with neuronal membranes. However, it has also found that the AD brain is characterized by an increase in oxidative stress. This research aims at a better understanding of this complex relationship by examining the effect of oxidizing selected glycine residues in Aβ42 on its potential toxicity and interaction with a lipid membrane containing the GM1 ganglioside. That would help toward better understanding of this neurodegenrative disorder and its treatment.

2.1 Effect of bilayer on Aβ42

2.1.1 Aβ42 Insertion Distance

To see which peptide residues most frequently interacted with the bilayer, we calculated the average distance between the COM of each residues and the average position of each lipid type along the bilayer normal (z-axis). The time-averaged z-position of the phosphorus atom of POPC was used as a reference by setting their average position to zero. The relative position of the hydroxyl oxygen of cholesterol and the COM of the GM1 head group are shown in Fig. 3. On average, the center of mass of the GM1 head groups are above the phosphate group of POPC, while the hydroxy group of cholesterol lay beneath it.

It can be seen in Fig. 3 and Fig. 4 that Aβ42-wt and Aβ42-GLR29 show similar bilayer interaction profiles, whereas both Aβ42-GLR25 and Aβ42-GLR33 had similar interaction profile. In the wild-type Aβ42 and Aβ42-GLR29, Asp1 is closest to the phosphate atoms of the POPC lipids. Its distance from POPC is around 0.5 nm in the former and 0.3 nm in the latter peptide. N-terminal residues Ala2 to Arg5 are the next closest to the bilayer in both cases. The residues in the central polar region (Ser26 to Lys28) were the furthest from the bilayer, whereas residues Ala30, Ile32, Val36, Gly37 from the C-terminal hydrophobic region

of the wt, and residues Lys16, Phe20 of Aβ42-GLR29 were the next furthest. Despite these similarities, Aβ42-GLR29 stays slightly closer to the bilayer than the wild-type Aβ42 does (see Fig. 4). In the case of Aβ42-GLR25 and Aβ42-GLR33, the former is on average the furthest from the bilayer and this is more pronounced in the N and C-terminal region. In the case of Aβ42-GLR25, the central polar region residues Glu22 to Gly29 are the furthest from the bilayer.

To analyze whether the binding of Aβ42 to the membrane has an effect on the membrane properties, we first calculated the average bilayer thickness based on the positions of the phosphorus atoms for each simulated system. The average bilayer thickness was found to be about 4.5 nm for all studied systems (see Table S1). This average value was then compared to the local bilayer thickness that was calculated for the snapshots of each trajectory where Aβ42 was bound to the membrane. To this aim, we utilized the GridMAT-MD tool (*68*, *69*) to calculate the local membrane thickness averaged over all HREMD snapshots containing at least one atom of Aβ42 within 0.5 nm of the lipid bilayer. The resulting 2D plots (Fig. S2) reveal a reduction in the local bilayer thickness to about 4.4 nm or even less upon the interaction of the peptide with the lipid head groups.

2.1.2 Aβ42 contacts and hydrogen bond with the bilayer

For a greater understanding of which Aβ42 residues associated with the bilayer, the number of contacts between each Aβ42 residue and the bilayer for the 4 systems were calculated and normalized in the range of 0 to 1, where 0 means that the residue made no contact with the lipid in question, and 1 stands for residues that always remained in contact with lipid (see Fig. 4).

The N-terminal residues of Aβ42-wt made the most contacts with POPC lipids. In this region Asp1 formed the most contacts, followed by Arg5, Glu3, and Ala2 respectively, then His6, Asp7 and Tyr10 from the metal binding region. Fewer contacts, with a normalized contact frequency of less than 0.2, were observed in the central polar and the C-terminal

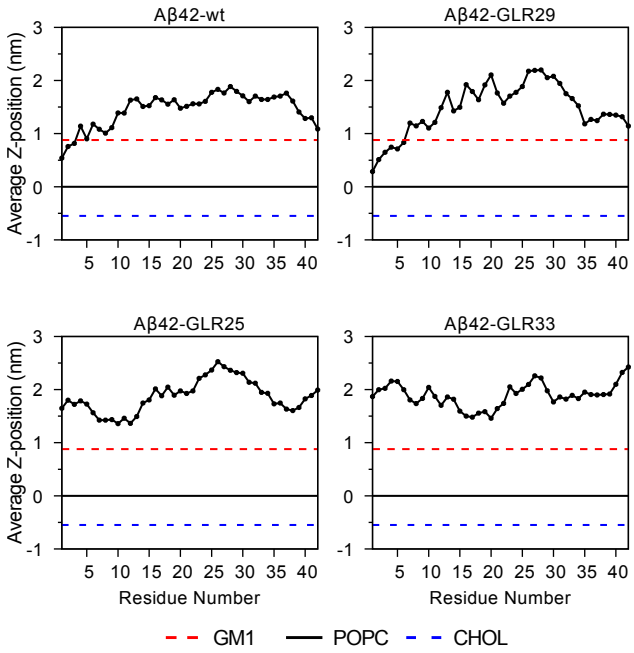

Figure 3: The average insertion distance of each Aβ42 residue with respect to the POPC and GM1 head groups and CHOL hydroxyl group. The head group of GM1, POPC, and CHOL are shown in red, black, and blue respectively.

hydrophobic regions. Similarly, the contacts between Aβ42-GLR29 residues and POPC were dominated by the N-terminal residues, with a higher membrane affinity shown here in this peptide residues than those in the wild-type. In this region the most contacts were made by Asp1 and the next highest is Ala2, followed by Arg5, Phe4 and Glu3 respectively, and then Tyr10 in the metal binding region. Fewer contacts (a normalized frequency of less than 0.2) were observed in the C-terminal region and almost no contacts were made between the bilayer and the central polar and central hydrophobic regions of the peptide. On the other hand, the contacts between Aβ42-GLR25 and POPC were dominated by residues from the metal binding region. In this region, contacts with residues Asp1, Arg5, Tyr10, Val12, His13 were most frequent. Fewer contacts, with a normalized frequency of less than 0.5, were observed among the remaining residues in this region and the C-terminal hydrophonic regions. Aβ42-GLR33 has the lowest affinity for POPC. The most contacts in this peptide were made by residues 13 to 17 from the metal-binding region, with a normalized frequency greater than 0.3.

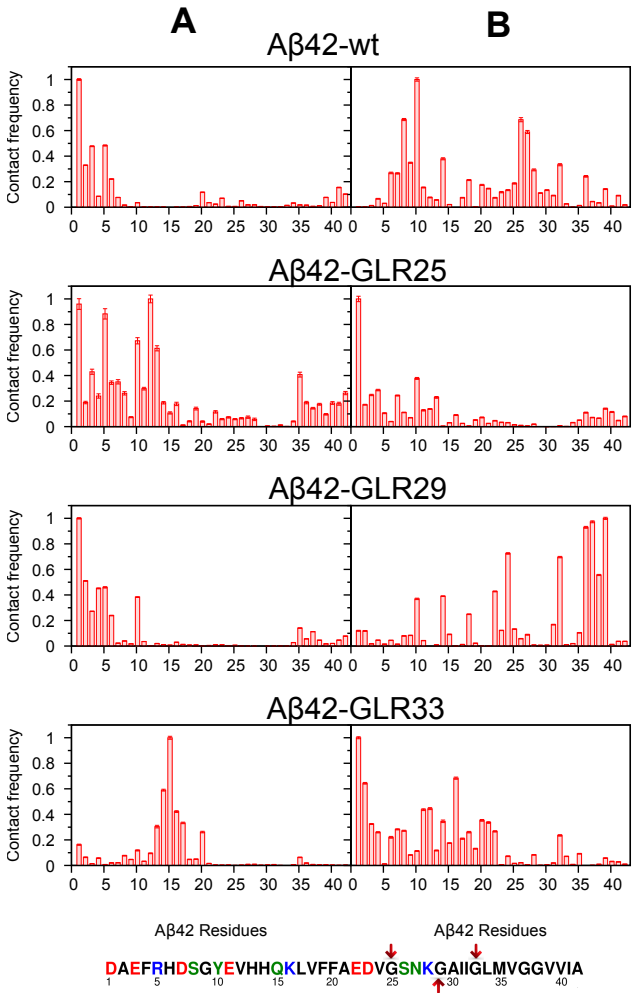

Figure 4: The contact frequency of each Aβ42 residue (and standard deviation of the mean) with POPC (A) and GM1 (B) head groups. The figure shows the normalized contact frequency in the range 0 to 1, such that 1 means the residue always made contacts with the lipid

, and zero means no contacts were made. The sequence of Aβ42 residues is shown below.

Most Aβ42 residues showed a propensity to bind GM1 in both the wt and oxidized peptides. However, the contact frequency in the metal-binding region is the highest in Aβ42-GLR33, followed by Aβ42-wt, Aβ42-GLR25, and Aβ42-GLR29. The central hydrophobic core and the central polar region had the highest affinity for GM1 in Aβ42-GLR33, followed by Aβ42-wt, Aβ42-GLR29 and Aβ42-GLR25 respectively. These contacts are almost abolished in the case of POPC. The C-terminal hydrophobic region showed the highest frequency to bind GM1 in Aβ42-GLR29 followed by Aβ42-wt, Aβ42-GLR33 and Aβ42-GLR25 respectively.

Residues Asp1 and Arg5 in the metal-binding region of Aβ42-wt and both Aβ42-GLR25 and GLR29 formed hydrogen bonds with POPC, as shown in Fig. 5. The propensity to form hydrogen bonds between Aβ42 and POPC is higher in the metal-binding region of Aβ42-wt and Aβ42-GLR29 than in Aβ42-GLR25, while it is less than 10% in some residues within the metal-binding region of Aβ42-GLR33. On the other hand, no hydrogen bonds formed between POPC and the central polar and C-terminal regions of any of the four Aβ42 peptides.

The propensity of hydrogen-bonds to form with GM1 is higher in the case of the oxidized Aβ42-GLR25, Aβ42-GLR29 and Aβ42-GLR33 than in the wt Aβ42. The C-terminal hydrophobic residues of Aβ42 tended to form hydrogen bonds with GM1, which was not the case with POPC. The highest hydrogen bond propensity of the C-terminal hydrophobic residues was observed in Aβ42-GLR29.

2.1.3 Aβ42 bilayer interaction energy

Next, we analyzed whether the contacts between Aβ42 residues and the lipid bilayer were driven by electrostatic or Lennard-Jones (LJ) interactions. The strongest Coulombic interactions (Fig. S3) between POPC and Aβ42-wt was at Asp1 at -256 kJ$\cdot$ mol^{-1}, and the next strongest interacting residue was Arg5, however the interaction strength at Arg5 was only 1/5 of that at Asp1. The Coulombic interactions between Aβ42-GLR29 and POPC showed

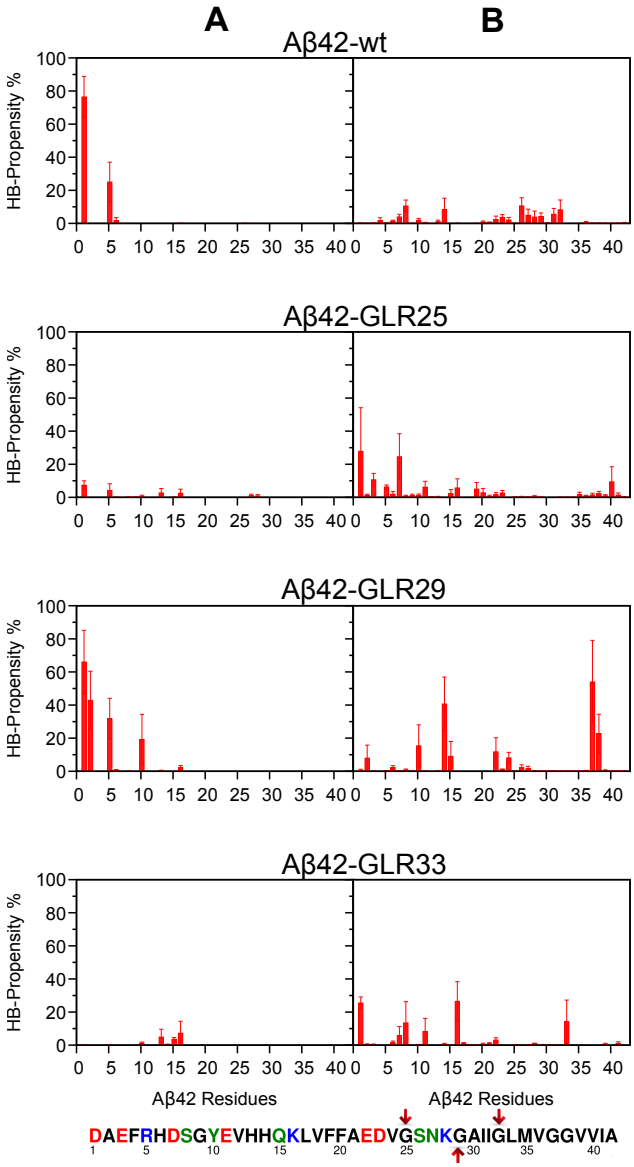

Figure 5: The hydrogen bond propensity (and standard deviation of the mean) of each Aβ42 residue with (A) POPC, and (B) GM1 head groups.

a similar trend as the wt but the interaction energy of Asp1 was weaker, at around -150 kJ$\cdot$ mol^{-1}, and around -20 kJ$\cdot$ mol^{-1} at Tyr10 compared to zero in the wt. The Coulombic interactions between POPC and Aβ42-GLR25 and Aβ42-GLR33 is less than -20 kJ$\cdot$ mol^{-1} with residues Asp1 in the former peptide and His13 to Lys16 in the latter peptide. The Coulombic interactions with GM1 was stronger in Aβ42-GLR25 and Aβ42-GLR33 compared to Aβ42-wt and Aβ42-GLR29. The strongest interaction was with Asp1 in Aβ42-GLR25 and with Lys16 in Aβ42-GLR33, and had interaction strengths of -104, and -60 kJ$\cdot$ mol^{-1}

respectively. The next strongest interaction between GM1 and Aβ42-GLR33 was with Asp1 at -50 kJ$\cdot$ mol^{-1}. Overall, the attractive Coulombic interactions with GM1 were lower in magnitude compared to those with POPC, where no single residue had an average interaction energy below -104 kJ$\cdot$ mol^{-1}.

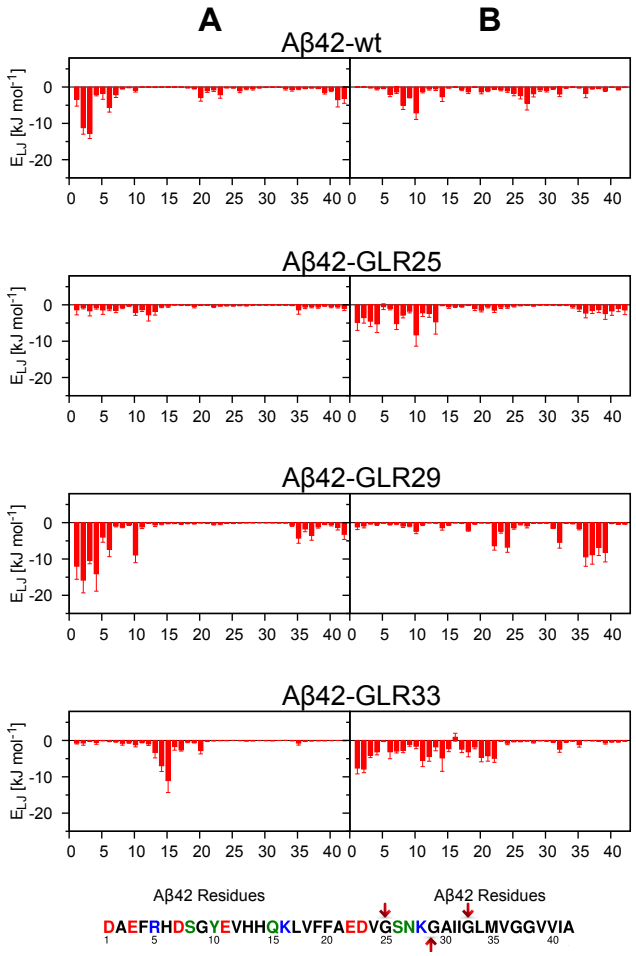

Figure 6: The Lennard-Jones interaction energy of each Aβ42 residue (and standard deviation of the mean) between Aβ42 and POPC (A) and GM1 (B) head groups.

The profile of the LJ interaction energies (Fig. 6) between each Aβ42 peptide and the lipids were very similar to that of their respective contact frequency figure (Fig. 4). For Aβ42-wt and Aβ42-GLR29 the strongest LJ interactions with POPC were in the N-terminal region of the peptides, and averaged between -10 and -13 kJ$\cdot$ mol^{-1}. In Aβ42-GLR33 the strongest LJ interactions were with residues His13 to Gln15, whereas residues in the central hydrophobic region averaged between -0.7 and -11 kJ$\cdot$ mol^{-1}. Similarly, the strongest LJ

interaction with GM1 was on average -10 kJ$\cdot$ mol^{-1} in the C-terminal region of Aβ42-GLR29 and both the metal binding and the central hydrophobic regions of Aβ42-GLR33. The LJ interactions of Aβ42-GLR25 with GM1 averaged less than -10 kJ$\cdot$ mol^{-1} and was dominated by residues from the metal binding and the C-terminal hydrophobic regions. It averaged less than -5 kJ$\cdot$ mol^{-1} in the the case of the wt Aβ42.

Furthermore, we examined the effect of solvation on peptide–lipid interactions, to assure that the stronger the peptide–lipid interaction the lesser the peptide is susceptible to solvation effects. To this aim, the time evolution of the number of water molecules within a 0.5 nm shell from the C-atom of the peptide (*70*, *71*) and the minimum distance of the peptide C_α atoms from the lipids were calculated and are jointly shown in Fig. S4. A decreasing peptide distance from the lipid (i.e. stronger peptide—lipid interactions) correlates with a reduction in the peptide hydration. Moreover, the highest population of solvating water molecules was present at approximately 3 nm distance of Aβ from the membrane surface, i.e., the initial distance and it takes around 50 ns for the peptide to move closer to the lipids.

2.2 Aβ42 structural properties

2.2.1 Aβ42 secondary structure assignment

In the wild-type Aβ, residues Phe4 to Glu11 displayed β-turn/bend structure. Residues Val12 to Gln15 displayed helical structure. Residues Lys16 to Ala21 showed a mixture of helical and β- turn/bend structure. Residues Glu22 to Val39 showed β-turn/bend structure with residues Ile32, Leu34, Val36 and Val39 displaying a mixture of β-strand/bridge and helical structure. Residues Met35, Val40, Ile41 showed β-strand/bridge.

Similar to what was seen in the wild-type, all oxidized Aβ peptides showed a high propensity to form a helical structure in the region Glu11 to Ala21 (Fig. 7), with the lowest propensity observed in the case of Aβ42-GLR25. However, an increase in helicity was observed in the case of Aβ42-GLR33, such that the helical region extended to include residues Asp7 to Ala21 from the central polar and central hydrophobic regions.

The propensity to form β-strand/bridge was the highest in Aβ42-GLR25 and Aβ42-wt. Few residues in Aβ42-GLR29 and Aβ42-GLR33 showed β-strand/bridge structure. This includes residues His6, Tyr10 in the former peptide and residues His13, Leu17, Gly29, Ala30, Val40, Ile41 in the latter peptide. On the other hand, all Aβ42 peptides showed a higher probability to form β-turn/bend. Interestingly, residues Asp23 to Asn27 in Aβ42-GLR25, residues Asn27 to Ile31 in Aβ42-GLR29 and residues Ile31 to Leu34 in Aβ42-GLR33 did not show any turn/bend structure.

Moreover, the development of the secondary structure content for all simulations as a function of the simulation time was analyzed and shown in Fig. S5. To this aim we utilized the moving window statistics (more about the method can be found in the figure caption) to test the convergence of the secondary structure during the simulation (*71*, *72*). The figure shows good agreement in the overall trend of the β-sheet propensity over different time windows, and the secondary structure propensity of the peptides apart from Aβ42-GLR25 converges after 80 ns as no further changes in the β-sheet propensity are observed by the end of the simulations. Aβ42-GLR25 is more flexible than the other three peptides, and thus needs more time for the secondary structure to converge. This is in line with the previous findings by Liao et. al. who found that the flexibility of Aβ42 increases upon oxidation of Gly25 (*65*). Nonetheless, within the last 40 ns of the HREMD simulation also this simulation converged as supported by the nearly stable β-sheet propensity for each of the residues.

2.2.2 Aβ42 intramolecular hydrogen bond and contact

Hydrogen bonds present within the peptide backbone, the peptide side chains, and between the peptide backbone and side chains that were present for more than 40% of the time were recorded and listed in Table S2. In the wild-type Aβ42, backbone-backbone hydrogen bonds were present in the C-terminal region between Ile41 with Gly33 and Leu34, Ile31 with Leu34 and Met35, Gly33 and Met35, Val36 and Val39, which stabilizes the β-sheet structure. They are also present between residues from the metal binding region such as Glu11 with

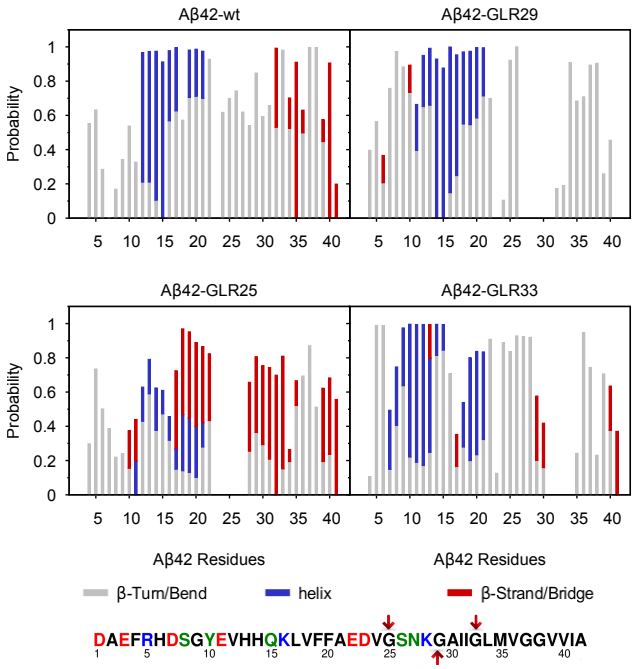

Figure 7: The secondary structure assignment of each Aβ42 residue in the case of Aβ42-wt, Aβ42-GLR25, Aβ42-GLR29, and Aβ42-GLR33 in a bilayer compromised of 70% POPC, 25% CHOL, 5% GM1. The β-turn/bend is shown in silver, the helix in blue and the β-strand/bridge is shown in red. The figure shows the additive probability of all secondary structure such that the maximum is 1, those residues showing probability lower than 1 form random coil.

His14 and Gln15, Val12 and Lys16, His14 with Leu17 and Val18, Val18 with Ala21 from the central hydrophobic region. In the N-terminal region, backbone-side chain hydrogen bonds formed between Glu3 with Phe4 and Arg5. Moreover, hydrogen bonds formed between the side chain of Glu3 (hydrogen bond acceptor) and the side chain of Arg5 (hydrogen bond donor) from this region. Similarly, a lower number of backbone-backbone hydrogen bonds were present in the Aβ42-GLR33 metal binding, and C-terminal regions. On the other hand, Aβ42-GLR29, and Aβ42-GLR25 contained additional backbone-backbone hydrogen bonds that formed within the central hydrophobic core, within the central polar region, and between the C-terminal and the central polar region in the former, and within the polar region, and between the C-terminal and the central hydrophobic cores of the latter. These bonds exist between residues that either form helices or β-sheets, and such structures are discussed in the next section about the most prevalent Aβ42 structures. Residues in the N-terminal region

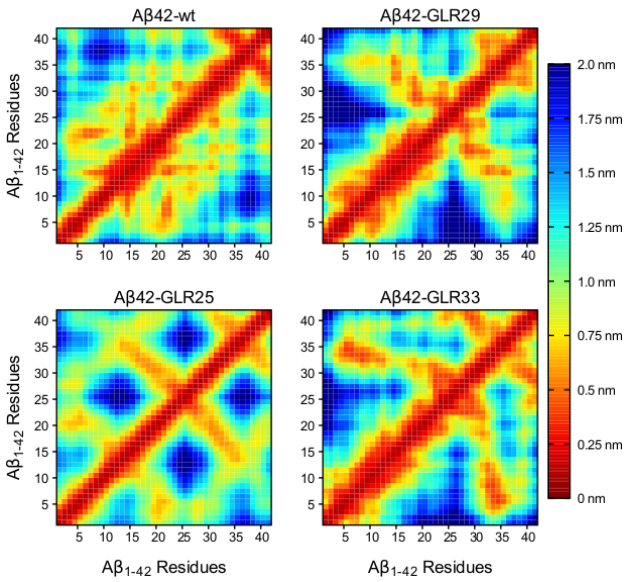

Figure 8: Contact map of each Aβ42 residue in the case of Aβ42-wt, Aβ42-GLR25, Aβ42-GLR29, and Aβ42-GLR33 in a bilayer compromised of 70% POPC, 25% CHOL, 5% GM1. The color box to the right shows the corresponding distance (in nm) to color present in the contact map.

did not form backbone to backbone hydrogen bonds in any of these peptides.

The backbone-side chain hydrogen bonds formed most often in Aβ42-GLR33. However, Phe4 formed hydrogen bond with Glu3 and Arg5 in all peptides except Aβ42-GLR25, which did not form any backbone-side chain hydrogen bonds. The hydrogen bonds involving side chains in Aβ42-GLR29 were similar to those observed in Aβ42-wt as is shown in Table S2. However, Aβ42-GLR33 formed an additional hydrogen bond between Ser26 and Asp23, and Aβ42-GLR25 did not form side chain to side chain hydrogen bonds.

The contact map between the Aβ42 residues is shown in Fig. 8. Regions marked in red indicates residues in close contact (within 0.25 nm of each other) and regions marked in blue stand for residues that display little to no contact. Based on this assignment one can explain the red main diagonal seen in all contact maps, as it represents the contact of a residue with itself and its neighboring residues. Of interest are those islands of red color that spread in almost all contact maps. Considering the contact map of Aβ42-GLR25, these light-orange-colored islands are arranged in cross diagonals between residues 28-34 with residues 14-24,

illustrating the formation of β-sheets. Similarly, these diagonals are observed in the other peptides but with some distortion and to a lesser degree in the following order Aβ42-GL29 > Aβ42-GL33 > Aβ42-wt.

2.2.3 The most prevalent Aβ42 structures

To substantiate the secondary structure and contact map analysis, we clustered the Aβ structures using the algorithm developed by Daura et al.. The top cluster of each system is presented in Fig. 9, while the structure in the second and third-largest cluster are shown in Fig. S7-S8. The three highest populated Aβ42-wt clusters represented 46.7%, 23.7%, and 9.5% of all structures respectively (Fig. 9A, Fig. S6A, and Fig. S7A). From the N-terminus to the C-terminus, the secondary structure of the largest and second-largest cluster alternated from random coil to turn, followed by helix at Val12 to Leu17, then a turn to anti-parallel β-sheet (on either sides of a turn centered at Gly38) at the C-terminal. There were no β-sheet in the third-largest cluster, however, Aβ42 contained coil, turn, and helix. The N-terminus was embedded more deeply into the bilayer in the largest and third-largest clusters, and was least embedded in the second-largest cluster. The three most populated structures found in Aβ42-GLR25 represented 33.8%, 18.4%, and 9.4% of all structures respectively are shown in Fig. 9B, Fig. S6B, and Fig. S7B. The β-sheet structure was observed only in the largest and second-largest clusters, however, a much higher β-sheet content can be seen in these clusters. In addition to the β-sheet at C-terminal, a β-sheet was observed at the central hydrophobic and polar region (residues Leu17 to Asp23, Lys28 to Leu34) in the largest cluster, and at the metal binding region (Gly9 to Val12) in the second-largest cluster. A helical structure was only observed in the second and the third largest clusters. The N terminus is closer to the bilayer in the largest cluster, while the the C-terminus is close to the bilayer in both the second and third-largest clusters. In the case of Aβ42-GLR29, the three representative structures representing 56.5%, 19.3%, and 3.8% of the total number of structures, respectively, are shown in Fig. 9C, Fig. S6C, and Fig. S7C. No β-sheets observed

in any of the three clusters. However, helical structure was seen in all clusters. Moreover, much more helical content was seen as the helical structure extends to include Glu11 to Glu22, and His13 to Ala21 in the second and the third-largest clusters respectively. The N-terminus is embedded in the bilayer in all three clusters, while the C-terminus is only embedded in the second-largest cluster. Fig. 9D, Fig. S6D, and Fig. S7D shows the three most populated structures in the presence of Aβ42-GLR33, which represent 65.6%, 16%, and 5.2% of the total structures respectively. In this case C-terminal β-sheet was observed only in the largest cluster. A helical structure observed in both the largest and second-largest cluster. There were no helices, no β-sheet in the third largest cluster. The N-terminus is close to the bilayer in the second-largest cluster, while both the N and C-terminus residues interact with the solvent in both the largest and the third-largest clusters.

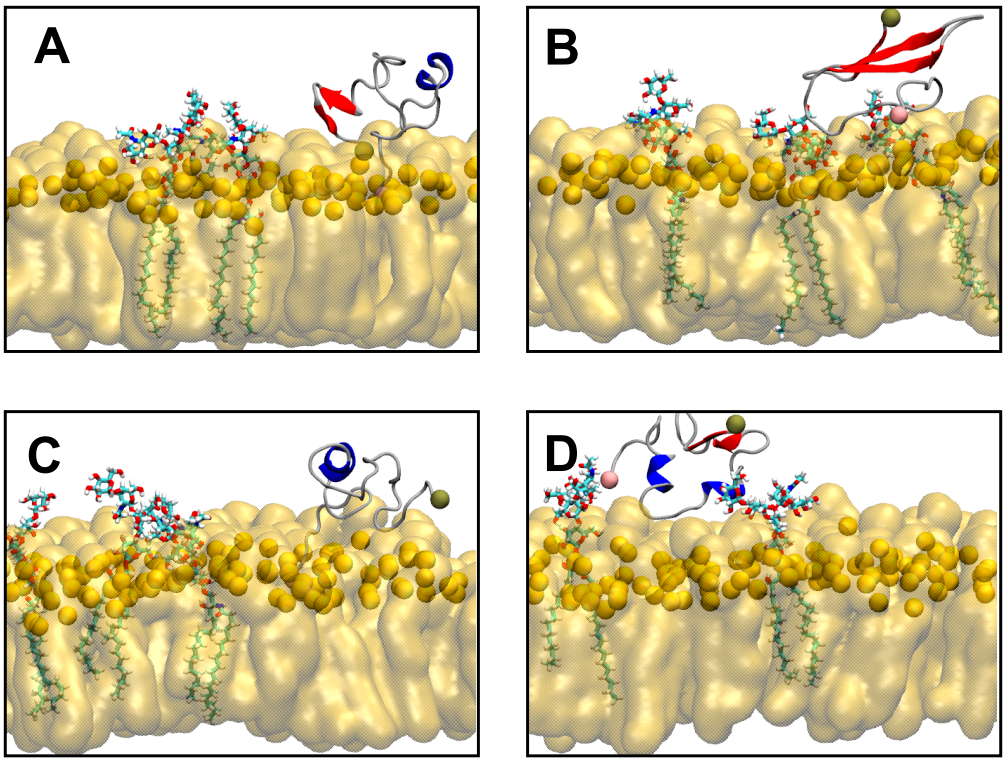

Figure 9: The central structure of the the largest cluster. (A) Aβ42-wt (46.7%), (B) Aβ42-GLR25 (33.8%), (C) Aβ42-GLR29 (56.5%), (D) Aβ42-GLR33 (65.6%). In each rendered image the lipids are colored by orange. The phosphate atom of POPC is in orange, the N and C terminals of Aβ42 are shown in pink and tan spheres respectively. The protein β sheet is in red, the helix is in blue, coil and turn are shown in silver.

2.3 Discussion

2.3.1 Effect of bilayer on Aβ42

The insertion data shows the time-averaged distance between each Aβ42 residue and the bilayer. The insertion depth of Aβ42-wt > Aβ42-GLR29 > Aβ42-GLR25 > Aβ42-GLR33, as characterized by the average insertion distance (Fig. 3). The detailed interactions of Aβ42 residues with the bilayer are shown more quantitatively in the peptide-bilayer contacts Fig. 4. Interactions between Aβ42 and the bilayer occur primarily between the N-terminus and the POPC head groups, while the remaining residues make more contact with GM1. Aβ42-GLR25 makes the least contact with GM1 as the normalized frequency is generally less than 0.5, which can indicate why it has the tendency to adopt the β-sheet conformation while on membrane surface. As shown in Fig. 4, the contact between peptides and GM1 are ranked in the order of Aβ42-GLR29> Aβ42-GLR33 > Aβ42-wt > Aβ42-GLR25. Contacts observed at the N-terminus especially with Asp1, and Arg5 were driven by hydrogen bonds that formed between the amino acid residues and the lipids. The propensity of hydrogen bonds to form between Aβ42 and GM1 are in the order of Aβ42-GLR29 > Aβ42-GLR33 > Aβ42-GLR25 > Aβ42-wt. The hydrogen bond propensity with POPC was limited to residues from the N-terminal metal-binding region, with Asp1 and Arg5 as the main hydrogen bond forming residues. This is expected to be the cause that drives the N-terminus to be close to the bilayer head group as can be seen from the insertion data in Fig. 3. Here, Aβ42-wt and Aβ42-GLR29 showed a higher hydrogen bond propensity with POPC than Aβ42-GLR25 and Aβ42-GLR33. It is not surprising that Aβ42 residues that form a hydrogen bond with the bilayer were also shown to be the strong energetic contribution to interactions between each peptide and the lipid bilayer. The interactions between each Aβ42 residue and the lipid bilayer were divided into their Coulombic and Lennard-Jones contributions. Overall, it can be seen from Figs. 6 and S3 that the Aβ–bilayer interaction are mostly hydrophobic in nature, since most residues interacted with the bilayer via Lennard-Jones interaction.

However, Coulombic interactions played a major role in the case of Asp1 and Arg5 residues in both Aβ42-wt and Aβ42-GLR29, which is expected due to their tendency to form hydrogen bonds with POPC.

The observation that Aβ42 formed most contacts with GM1 can be attributed to the large head group of GM1 containing five sugar groups (Fig. S8) that tend to lay on the membrane surface, thus providing a platform for hydrogen bonding with Aβ42 through its sugar head groups (Fig. 4). It should be noted that with 5% GM1 in the bilayer there were only 7 GM1 lipids in each leaflet. Despite this low GM1 content, as can be seen from the most populated clusters (Figs. 9, S6 and S7), Aβ42 has a preference to bind to GM1 and in some cases even to two GM1 molecules at the same time due to the possibility of hydrogen bonding to the penta-saccharide GM1 head group. In order to further elucidate the Aβ42–GM1 binding, we dissected these interactions into their contributions per sugar ring. The representative snapshot in Fig. S9 and the contact probability in Fig. S10 show that independent of the oxidation state of Aβ42, the peptide made most contacts with the sugar groups furthest away from the membrane surface, that is the terminal β-D-Galactose (Gal'), the N-acetyl-β-D-galactosamine (GalNAc), and the N-aceytl-αneuraminidate (Neu). Apart from Aβ42-GLR25, the other three Aβ42 variants preferred binding to Neu, while Aβ42-GLR25 formed more contacts with Gal'. The contact probability of Aβ42-wt and Aβ42-GLR25 with GalNAc is also considerably high, leading to some contacts with the adjacent Gal, while Aβ42-GLR29 and Aβ42-GLR33 formed only few contacts with GalNAc. Fig. S11 confirms that in all cases the contacts between Aβ42 and the sugar groups are driven by hydrogen-bond formation, which, however, does not only involve Coulomb but also Lennard-Jones interactions (Fig. S12). The formation of hydrogen bonds of Aβ42 with GM1 prevents the peptide from forming intrapeptide hydrogen bonds as needed for secondary structure formation, e.g., the formation of β-sheets and α-helices. This is indeed the case as the numerous snapshots in Figs. 9, S6 and S7 reveal: at the Aβ42–GM1 binding sites, no β-sheet or α-helix is found. However, the binding of Aβ42 to GM1 keeps Aβ42, or at least

parts of it somewhat above the membrane surface (Fig. 3), which in turn encourages β-sheet formation as seen for Aβ42-GLR25 in Fig. 9B or helix formation as observed for Aβ42-GLR29 and Aβ42-GLR33 in Fig. 9C and D. The higher amount of structure formation of membrane-associated Aβ42 compared to the solution state can thus be considered to be a consequence of the reduction in conformational flexibility on the membrane surface, while leaving Aβ42 enough conformational freedom and also possibilities for intrapeptide hydrogen-bond formation needed for β-sheet or helix formation.

2.3.2 Effect on Aβ42 secondary structure

The secondary structure of Aβ42 has similar secondary structure elements in each system, particularly in the helical central polar region (Val12 to Ala21). This region remained helical in all peptides, though it is extended to include residues Asp7 to Ala21 in Aβ42-GLR33. As evidenced by the membrane contacts, hydrogen bonding, and interaction energies the conformation of Aβ42 in the N-terminal region was not affected by the interaction with POPC. This is because Aβ42-GLR25 showed higher contact frequency with POPC in the N-terminal compared to Aβ42-GLR33, however both peptides showed no tendency to form β-sheets in the N-terminal region. The same is applied to Aβ42-GLR29 and Aβ42-wt. On the other hand, the interaction with GM1 affected the formation of β-sheets. It was observed that Aβ42-GLR29 and Aβ42-GLR33 showed the highest number of contacts with GM1 when compared to Aβ42-wt and Aβ42-GLR25, but these peptides had a lower tendency to form β-sheets, which is in agreement with the finding of Mandel et al. on Aβ40 (*73*). This is also confirmed by the insertion data (Fig. 3) which shows that Aβ42-wt and Aβ42-GLR25 behave differently with respect to the bilayer, with both pepides having a lower tendency to bind to GM1 (Fig. 4) than Aβ42-GLR29 and Aβ42-GLR33 does.

The assignment of secondary structure is shown in Fig. 7 and it mirrors what is seen in the most populated clusters Fig. 9. The intra-peptide backbone hydrogen bonds indicate a structure that is very similar to that of a β-sheet in the most populated clusters for these

two systems.

2.3.3 Comparison with other studies

It is known from experimental findings and MD simulations that Aβ42 is an intrinsically disordered protein, containing all possible secondary structures (*9*, *74*–*77*). It has also been shown that the C-terminal β-sheet is the seed for further Aβ aggregation into β-sheet rich structure (*74*). Moreover, the importance of the total β-strand content for controlling the aggregation rates was pointed out in an MD study by Man et al. (*78*). In our study we observed a C-terminal β-sheet in the case of Aβ42-wt and Aβ42-GLR25 especially in the two regions, Val39-Ile41 and Ala30-Val36. We also found that there is a β-sheet forming propensity in the region of Leu17 to Glu22 and Tyr10 to Glu11 in Aβ42-GLR25. However the β-sheet forming propensity in the C-terminal hydrophobic region was very low in the cases of Aβ42-GLR29 and Aβ42-GLR33, which might be explained by the findings of Fonte et al. (*53*) and Harmeier et al. (*54*). Fonte et al. found experimentally that changes in the glycine zipper Gly29-XXX-Gly33-XXX-Gly37 motif prevent the formation of toxic oligomers as they observed a reduction in Aβ toxicity upon the substitution of Gly37 with leucine (*53*). It was also found by Harmeier et al. that the substitution of Gly33, which is both at the end of one and at the start of the next GXXXG interaction motif, causes the formation of less toxic oligomers. Based on that, we suggest that the stability of the C-terminal β-sheet in Aβ42-GLR25 might be attributed to the fact that Gly25 does not disrupt the zipper motif.

According to our findings, the effect of radicalization of Gly residue on the structure of Aβ42 depends on the position of the oxidized Gly residue within the C-terminal hydrophobic region of Aβ. This is supported by the MD study of Owen and coworkers on three fast folding miniproteins, where it was also found that denaturing effect of the Gly radicals depended on the position of the radical (*64*). Structural changes in the protein upon Gly oxidation were more pronounced in the α-helix rich protein than the β-sheet rich one due to the flat geoemtry of the radical (Fig. S1) (*64*). This may even cause the formation of a β-sheet as

Owen et al. showed in an MD-study of a short helical peptide that underwent a transition to a β-sheet conformation upon radical formation (*63*).

It has been shown experimentally that Aβ interacts strongly with lipid bilayers compromised of phosphatidylcholine head groups (*79*, *80*). In our study we found that this interaction is mediated by hydrogen bonds with the positively charged N-terminal Asp1 and the side chain of Arg5. Furthermore, we found that such tight interactions have no effect on Aβ secondary structure, which is in agreement with the experimental findings that binding of Aβ to PC-containing bilayers does not affect the secondary structure of the Aβ peptide at low concentrations (*81*, *82*). Our results showed how the bulky GM1 head groups covers a large area of the membrane even with only 7 GM1 lipids in each bilayer leaflet, and the peptide is more likely to bind to the GM1 head groups, especially to the terminal saccharide residues, than to the POPC head groups. This agrees with the findings by Manna et al. who concluded that the GM1 head groups act as scaffold for Aβ binding through sugar-specific interactions (*83*). They further observed the formation of a C-terminal β-hairpin upon binding of Aβ42 to GM1, which is also in line with our results. However, it should be noted that another study found that binding of Aβ40 to GM1 head groups induces the formation of a helix on the C-terminal side of the peptide (*84*). We also observed helix formation upon GM1 binding, which, however, occurred preferentially between residues 10 and 21 of Aβ42. This includes the region from 17 to 21 that was already identified as helical for Aβ40 in solution (*85*). From an experimental study it was followed that low concentrations of GM1, i.e. physiological concentration of GM1 that range from 2–4% of the total lipid content of the membrane (*86*), enhance the formation of β-sheets, but prevents Aβ oligomerization (*87*). Other experiments further showed that the higher the concentrations of GM1 (but less physiologically relevant), the higher the β-sheet content of Aβ becomes (*88*).

3 Methods

3.1 Model System and System Equilibration

The starting structures for the wild-type (wt) and oxidized (Gly25, Gly29, Gly33) Aβ peptides were obtained from 1 μs simulations, using the final snapshots of these simulations (Fig. S13). These simulations had begun with the structure of Aβ42 as determined by NMR spectroscopy (PDB ID: 1Z0Q) (*89*). The N- and C-terminals were the free amino ($NH3^+$) and carboxyl (COO^-) groups, respectively, and thus each peptide carried an overall charge of -3. The oxidized Aβ42 peptides will be henceforth referred to as Aβ42-GLR25, Aβ42-GLR29 and Aβ42-GLR33. The four peptides were placed 3.5 nm above a symmetric membrane composed of 202 POPC, 72 CHOL and 14 GM1 lipids. Each system was solvated with TIP3P water model (*90*) and neutralized with 17 Na^+ ions. In addition, 150 mM of NaCl were added to mimic the physiological concentration of these ions. The exact numbers of each molecules present in each system are listed in Table 1. All interactions among system constituents were described using OPLS-AA force field parameters (*66*, *91–93*). All MD simulations carried out using GROMACS 4.6 simulation package (*94*).

The systems were energy minimized using the steepest descent algorithm to remove all atomic clashes (*95*, *96*). This was followed by an equilibration under NVT conditions for 1 ns, where the reference temperature of 310 K was regulated with the velocity-rescale thermostat (*97*) and the time constant set to 0.1 ps. During minimization and initial equilibration stages, the heavy atoms of protein and lipids were subjected to position restraints with a force constant of 1000 kJ/mol$\cdot$ nm^2. Next, the system was equilibrated under NPT conditions for 10 ns to obtain a pressure of 1.0 bar. The pressure was regulated using semi-isotropic Parrinello-Rahman pressure coupling scheme (*98–100*) with a time constant of 5 ps and isothermal compressibility of 4.5e-5 bar^{-1}. The temperature of 310 K was maintained with Nosé-Hoover thermostat (*101–104*) with a time constant of 0.5 ps, while the position restraints on the protein and lipids were still on. The particle Mesh Ewald (PME) (*105*, *106*)

method was used to account for the electrostatic interactions within the system. Both the short-range interactions, with a van der Waals cutoff of 1.0 nm (real space), and the long-range (Fourier) electrostatics were used under the periodicity assumption, and the periodic boundary conditions were set in all directions. All bonds were constrained using LINCS algorithm (*107*).

3.2 Hamiltonian Replica Exchange MD (HREMD) Simulations

For the final production run, the input parameters were the same as those under NPT conditions, except that the position restraints were switched off. To accelerate conformational sampling, we employed the HREMD protocol for the systems described in the previous section using the protocol introduced in (*108*). System coordinates and input parameters (without restraints) from the NPT equilibration served as the initial input to generate the post-processed topology files required for the HREMD simulations. The system was split into hot (Aβ peptide) and cold (the rest of the system) regions, where the interactions within the hot region and between the hot region and the cold region was enhanced by scaling the force field terms for the proper dihedrals, Lennard-Jones parameters and electrostatic interactions. HREMD simulations were performed using 14 replicas with λ values ranging from 1 to 0.5 and replica exchanges were attempted every 2 ps. Each system was simulated for 200 ns per λ value with the exchange acceptance ratio of 0.13. All simulations were carried out with GROMACS 4.6 patched to PLUMED 2.2. (*109*).

3.3 Analysis methods

3.3.1 Bilayer-peptide interactions

The analysis of each system began when Aβ was within 0.5 nm of the bilayer. All analysis programs mentioned in this section are included in the GROMACS 2018.2 program package (*110–113*). The 'gmx traj' program was used to measure the insertion distance of Aβ42

by computing the center of mass (COM) of each residue and the average vertical position of the phosphorus atoms of phospholipids was taken along the z-axis. The 'gmx mindist' program was employed to determine the number of contacts between each Aβ42 residue and each POPC or GM1 lipid. A contact was recorded when the distance between any two non-hydrogen atoms from the residue and lipid in question was within 0.5 nm. Then the number of contacts were normalized in the range of 0 to 1. The hydrogen bond propensity was determined by the number of times a hydrogen bond was formed between hydrogen bond donating and accepting atoms in Aβ42 and each lipid type using the 'gmx hbond' program. A hydrogen bond was recorded when the angle between the donor and acceptor bonded hydrogen was between 150 and 180 degrees and the distance between the two atoms was within 0.35 nm. The 'gmx energy' program was used to calculate the interactions energy between each Aβ residue and the head group of POPC or GM1.

Table 1: The molecular composition of the four membrane systems; Aβ42-wt, Aβ42-GLR25, Aβ42-GLR29, and Aβ42-GLR33.

	Number of molecules						
	Peptide	Lipids			Ions		Water
Bilayer system	Aβ42	POPC	CHOL	GM1	Na^+	Cl^-	
Aβ42-wt	1	202	72	14	69	52	19301
Aβ42-GLR25	1	202	72	14	69	52	19289
Aβ42-GLR29	1	202	72	14	69	52	19293
Aβ42-GLR33	1	202	72	14	69	52	19259

3.3.2 Aβ42 structure

The secondary structure of each Aβ42 residue was determined using the *define secondary structure program* (do_dssp) (*114*). To facilitate a clear representation, the data of similar secondary structures are grouped together; β-strand and β-bridge are combined as β-strand/bridge, β-turn and bend as β-turn/bend and helix includes α, π, and 3_{10} helices. Hydrogen bonds within the peptide backbone, between the backbone and side chains, and between the side chains were counted by applying the same method used for counting the

peptide-lipid hydrogen bonds. Representative Aβ42 structures were obtained by the 'gmx cluster' program using the method of Daura et al. (*115*) and a cutoff of 0.25 nm for clustering. The conformation and membrane interactions of the central structure of the three largest clusters were rendered using the VMD program (*116*).

4 Conclusion

Understanding the interplay between oxidative stress and Aβ neurotoxicity requires exploring the conformation of oxidized Aβ peptides. Based on our MD simulations of Aβ42 and its oxidized variants in interplay with a model membrane bilayer we found that Aβ42-GLR25 is potentially as toxic as Aβ42-wt, assuming that β-sheet formation in Aβ is connected to its toxicity (*12*), whereas Aβ42-GLR29 and Aβ42-GLR33 showed less β-sheet forming propensity. We also revealed that the sugar moiety of GM1 affects the interaction between Aβ42 and the membrane. Aβ has a high tendency to interact with GM1 (especially Aβ42-GLR29 and Aβ42-GLR33), and once this happens the propensity of the peptide to form β-sheet is greatly reduced as Aβ, instead forming intrapeptide hydrogen bonds, interacts with GM1 through hydrogen bonds. Moreover, the interaction with GM1 also reduces the number of contacts and hydrogen bonds that the peptide makes with POPC. On the other hand, the insertion of the peptide into the bilayer is enhanced by its interaction with POPC; Aβ42-wt and Aβ42-GLR29 showed the highest number of contacts with POPC and therefore these peptides interact most closely with the bilayer. Our results suggest that the differences observed in Aβ conformation and interaction with the bilayer upon the oxidation of different glycine residues might be attributed in part to the position of these residues within the C-terminal hydrophobic region of Aβ and its subsequent interaction with GM1. Further studies should test this observation and further determine the role of oxidation in Aβ-mediated AD toxicity.

5 Author Contributions

All authors made a significant contribution to this manuscript. The contribution of each author is as follows:

H. Fatafta: Analyzed simulation data, prepared figures and presented data, wrote manuscript.

C. Poojari : Designed the study, set-up simulations, wrote manuscript.

A. Sayyed-Ahmad : Provided study funding, wrote manuscript.

B. Strodel: Provided study funding, interpreted simulation data, wrote manuscript.

M. Owen : Designed study, provided study funding, carried out simulations, wrote manuscript.

Acknowledgement

H. F., A. S.-A. and B. S. acknowledge funding for this project from the Palestinian-German Science Bridge financed by the German Federal Ministry of Education and Research (BMBF). H. F. and B. S. gratefully acknowledge the computing time granted through JARA-HPC (project JICS6C) on the supercomputer JURECA at Forschungszentrum Jülich. This project has received funding from the European Union's Horizon 2020 research and innovation programme under the Marie Skłodowska-Curie grant agreement no. 665860 and it is co-financed by the South Moravian Region. This article reflects only the author's (M. C. O.) view and the EU is not responsible for any use that may be made of the information it contains. M C. O, also thanks the Helmholtz Postdoc Programme. Access to computing and storage facilities owned by parties and projects contributing to the National Grid Infrastructure MetaCentrum provided under the programme "Projects of Large Research, Development, and Innovations Infrastructures" (CESNET LM2015042) is greatly appreciated.

Supporting Information Available

The supporting information is available at .... It includes explanation figures and table that further explain the structure used in this study and enhance our analysis.

References

1. Burns, A., and Iliffe, S. (2009) Alzheimer's disease. *Br. Med. J. 338*, 467–471.

2. Förstl, H., and Kurz, A. (1999) Clinical features of Alzheimer's disease. *Eur. Arch. Psy. Clin. N. 249*, 288–290.

3. Niu, Z., Zhang, Z., Zhao, W., and Yang, J. (2018) Interactions between amyloid β peptide and lipid membranes. *Biochim. Biophys. Acta, Biomembr. 1860*, 1663–1669.

4. Rangachari, V., Dean, D. N., Rana, P., Vaidya, A., and Ghosh, P. (2018) Cause and consequence of Aβ–Lipid interactions in Alzheimer disease pathogenesis. *Biochim. Biophys. Acta, Biomembr. 1860*, 1652–1662.

5. Cheng, Q., Hu, Z.-W., Doherty, K. E., Tobin-Miyaji, Y. J., and Qiang, W. (2018) The on-fibrillation-pathway membrane content leakage and off-fibrillation-pathway lipid mixing induced by 40-residue β-amyloid peptides in biologically relevant model liposomes. *Biochim. Biophys. Acta, Biomembr. 1860*, 1670–1680.

6. Owen, M. C., Gnutt, D., Gao, M., Wärmländer, S. K., Jarvet, J., Gräslund, A., Winter, R., Ebbinghaus, S., and Strodel, B. (2019) Effects of in vivo conditions on amyloid aggregation. *Chem. Soc. Rev. 48*, 3946–3996.

7. Hardy, J. A., and Higgins, G. A. (1992) Alzheimer's disease: the amyloid cascade hypothesis. *Science 256*, 184–186.

8. Cheng, R. P., Gellman, S. H., and DeGrado, W. F. (2001) β-Peptides: from structure to function. *Chem. Rev. 101*, 3219–3232.

9. Lührs, T., Ritter, C., Adrian, M., Riek-Loher, D., Bohrmann, B., Döbeli, H., Schubert, D., and Riek, R. (2005) 3D structure of Alzheimer's amyloid-β (1–42) fibrils. *Proc. Natl. Acad. Sci. U. S. A. 102*, 17342–17347.

10. Kael, M. A., Weber, D. K., Separovic, F., and Sani, M.-A. (2018) Aggregation kinetics in the presence of brain lipids of Aβ (1–40) cleaved from a soluble fusion protein. *Biochim. Biophys. Acta, Biomembr. 1860*, 1681–1686.

11. Marshall, K. E., Vadukul, D. M., Dahal, L., Theisen, A., Fowler, M. W., Al-Hilaly, Y., Ford, L., Kemenes, G., Day, I. J., Staras, K., and Serpell, L. C. (2016) A critical role for the self-assembly of Amyloid-β1-42 in neurodegeneration. *Sci. Rep. 6*, 30182.

12. Ono, K., Condron, M. M., and Teplow, D. B. (2009) Structure–neurotoxicity relationships of amyloid β-protein oligomers. *Proc. Natl. Acad. Sci. U. S. A. 106*, 14745–14750.

13. El-Agnaf, O. M., Mahil, D. S., Patel, B. P., and Austen, B. M. (2000) Oligomerization and toxicity of β-amyloid-42 implicated in Alzheimer's disease. *Biochem. Biophys. Res. Commun. 273*, 1003–1007.

14. Petkova, A. T., Ishii, Y., Balbach, J. J., Antzutkin, O. N., Leapman, R. D., Delaglio, F., and Tycko, R. (2002) A structural model for Alzheimer's β-amyloid fibrils based on experimental constraints from solid state NMR. *Proc. Natl. Acad. Sci. U. S. A. 99*, 16742–16747.

15. Kim, W., and Hecht, M. H. (2006) Generic hydrophobic residues are sufficient to promote aggregation of the Alzheimer's Aβ42 peptide. *Proc. Natl. Acad. Sci. U. S. A. 103*, 15824–15829.

16. Cukalevski, R., Boland, B., Frohm, B., Thulin, E., Walsh, D., and Linse, S. (2012) Role of aromatic side chains in amyloid β-protein aggregation. *ACS Chem. Neurosci. 3*, 1008–1016.

17. Poojari, C., Kukol, A., and Strodel, B. (2013) How the amyloid-β peptide and membranes affect each other: An extensive simulation study. *Biochim. Biophys. Acta, Biomembr. 1828*, 327–339.

18. Poojari, C., and Strodel, B. (2013) Stability of transmembrane amyloid β-peptide and membrane integrity tested by molecular modeling of site-specific Aβ42 mutations. *PLoS One 8*, No. e78399.

19. Varadarajan, S., Yatin, S., Aksenova, M., and Butterfield, D. A. (2000) Alzheimer's amyloid β-peptide-associated free radical oxidative stress and neurotoxicity. *J. Struct. Biol. 130*, 184–208.

20. Butterfield, D. A., and Lauderback, C. M. (2002) Lipid peroxidation and protein oxidation in Alzheimer's disease brain: potential causes and consequences involving amyloid β-peptide-associated free radical oxidative stress. *Free Radical Biol. Med. 32*, 1050–1060.

21. Drake, J., Link, C. D., and Butterfield, D. A. (2003) Oxidative stress precedes fibrillar deposition of Alzheimer's disease amyloid β-peptide (1–42) in a transgenic Caenorhabditis elegans model. *Neurobiol. Aging 24*, 415–420.

22. Butterfield, D. A. (2004) Proteomics: a new approach to investigate oxidative stress in Alzheimer's disease brain. *Brain Res. 1000*, 1–7.

23. Sultana, R., and Butterfield, D. A. (2010) Role of oxidative stress in the progression of Alzheimer's disease. *J. Alzheimer's Dis. 19*, 341–353.

24. Huang, W.-J., Zhang, X., and Chen, W.-W. (2016) Role of oxidative stress in Alzheimer's disease. *Biomed. Rep. 4*, 519–522.

25. Brown, D. R. (2005) Neurodegeneration and oxidative stress: prion disease results from loss of antioxidant defence. *Folia Neuropathol. 43*, 229–243.

26. Cheignon, C., Tomas, M., Bonnefont-Rousselot, D., Faller, P., Hureau, C., and Collin, F. (2018) Oxidative stress and the amyloid beta peptide in Alzheimer's disease. *Redox Biol. 14*, 450–464.

27. Smith, D. G., Cappai, R., and Barnham, K. J. (2007) The redox chemistry of the Alzheimer's disease amyloid β peptide. *Biochim. Biophys. Acta, Biomembr. 1768*, 1976–1990.

28. Zhao, Y., and Zhao, B. (2013) Oxidative stress and the pathogenesis of Alzheimer's disease. *Oxid. Med. Cell. Longevity 2013*, No. 316523.

29. Minicozzi, V., Stellato, F., Comai, M., Dalla Serra, M., Potrich, C., Meyer-Klaucke, W., and Morante, S. (2008) Identifying the minimal copper-and zinc-binding site sequence in amyloid-β peptides. *J. Biol. Chem. 283*, 10784–10792.

30. Marino, T., Russo, N., Toscano, M., and Pavelka, M. (2010) On the metal ion (Zn^{2+}, Cu^{2+}) coordination with beta-amyloid peptide: DFT computational study. *Interdiscip. Sci.: Comput. Life Sci. 2*, 57–69.

31. Roberts, B. R., Ryan, T. M., Bush, A. I., Masters, C. L., and Duce, J. A. (2012) The role of metallobiology and amyloid-β peptides in Alzheimer's disease. *J. Neurochem. 120*, 149–166.

32. Pearson, H. A., and Peers, C. (2006) Physiological roles for amyloid β peptides. *J. Physiol. (Oxford, U. K.) 575*, 5–10.

33. Brothers, H. M., Gosztyla, M. L., and Robinson, S. R. (2018) The Physiological Roles of Amyloid-β Peptide Hint at New Ways to Treat Alzheimer's Disease. *Front. Aging Neurosci. 10*, 118.

34. Michikawa, M., Gong, J.-S., Fan, Q.-W., Sawamura, N., and Yanagisawa, K. (2001)

A novel action of Alzheimer's amyloid β-protein (Aβ): oligomeric Aβ promotes lipid release. *J. Neurosci. 21*, 7226–7235.

35. Koudinova, N. V., Koudinov, A. R., and Yavin, E. (2000) Alzheimer's Aβ1–40 Peptide Modulates Lipid Synthesis in Neuronal Cultures and Intact Rat Fetal Brain Under Normoxic and Oxidative Stress Conditions. *Neurochem. Res. 25*, 653–660.

36. Yanagisawa, K., Odaka, A., Suzuki, N., and Ihara, Y. (1995) GM1 ganglioside–bound amyloid β–protein (Aβ): A possible form of preamyloid in Alzheimer's disease. *Nat. Med. (N. Y., NY, U. S.) 1*, 1062.

37. Di Scala, C., Chahinian, H., Yahi, N., Garmy, N., and Fantini, J. (2014) Interaction of Alzheimer's β-amyloid peptides with cholesterol: mechanistic insights into amyloid pore formation. *Biochemistry 53*, 4489–4502.

38. Kakio, A., Nishimoto, S.-i., Yanagisawa, K., Kozutsumi, Y., and Matsuzaki, K. (2002) Interactions of amyloid β-protein with various gangliosides in raft-like membranes: importance of GM1 ganglioside-bound form as an endogenous seed for Alzheimer amyloid. *Biochemistry 41*, 7385–7390.

39. Thomaier, M., Gremer, L., Dammers, C., Fabig, J., Neudecker, P., and Willbold, D. (2016) High-affinity binding of monomeric but not oligomeric amyloid-β to ganglioside GM1 containing nanodiscs. *Biochemistry 55*, 6662–6672.

40. Di Scala, C., Yahi, N., Boutemeur, S., Flores, A., Rodriguez, L., Chahinian, H., and Fantini, J. (2016) Common molecular mechanism of amyloid pore formation by Alzheimer's β-amyloid peptide and α-synuclein. *Sci. Rep. 6*, 28781.

41. Eckert, G. P., Kirsch, C., Leutz, S., Wood, W. G., and Müller, W. E. (2003) Cholesterol modulates amyloid beta-peptide's membrane interactions. *Pharmacopsychiatry 36*, 136–143.

42. Fantini, J., Yahi, N., and Garmy, N. (2013) Cholesterol accelerates the binding of Alzheimer's β-amyloid peptide to ganglioside GM1 through a universal hydrogen-bond-dependent sterol tuning of glycolipid conformation. *Front. Physiol 4*, 120.

43. Cui, Z. J., Han, Z. Q., and Li, Z. Y. (2012) Modulating protein activity and cellular function by methionine residue oxidation. *Amino Acids 43*, 505–517.

44. Butterfield, D. A., and Kanski, J. (2002) Methionine residue 35 is critical for the oxidative stress and neurotoxic properties of Alzheimer's amyloid β-peptide 1–42. *Peptides 23*, 1299–1309.

45. Butterfield, D. A., and Boyd-Kimball, D. (2005) The critical role of methionine 35 in Alzheimer's amyloid β-peptide (1–42)-induced oxidative stress and neurotoxicity. *Biochim. Biophys. Acta, Proteins Proteomics 1703*, 149–156.

46. Butterfield, D. A., and Sultana, R. (2011) Methionine-35 of Aβ (1–42): importance for oxidative stress in Alzheimer disease. *J. Amino Acids 2011*, No. 198430.

47. Boyd-Kimball, D., Sultana, R., Mohmmad-Abdul, H., and Butterfield, D. A. (2005) Neurotoxicity and oxidative stress in D1M-substituted Alzheimer's Aβ (1-42): relevance to N-terminal methionine chemistry in small model peptides. *Peptides 26*, 665–673.

48. Varadarajan, S., Kanski, J., Aksenova, M., Lauderback, C., and Butterfield, D. A. (2001) Different Mechanisms of Oxidative Stress and Neurotoxicity for Alzheimer's Aβ (1- 42) and Aβ (25- 35). *J. Am. Chem. Soc. 123*, 5625–5631.

49. Varadarajan, S., Yatin, S., Kanski, J., Jahanshahi, F., and Butterfield, D. A. (1999) Methionine residue 35 is important in amyloid β-peptide-associated free radical oxidative stress. *Brain Res. Bull. 50*, 133–141.

50. Kanski, J., Varadarajan, S., Aksenova, M., and Butterfield, D. A. (2002) Role of glycine-

33 and methionine-35 in Alzheimer's amyloid β-peptide 1–42-associated oxidative stress and neurotoxicity. *Biochim. Biophys. Acta, Mol. Basis Dis. 1586*, 190–198.

51. Rauk, A., Armstrong, D. A., and Fairlie, D. P. (2000) Is oxidative damage by β-amyloid and prion peptides mediated by hydrogen atom transfer from glycine α-carbon to methionine sulfur within β-sheets? *J. Am. Chem. Soc. 122*, 9761–9767.

52. Mazzitelli, S., Filipello, F., Rasile, M., Lauranzano, E., Starvaggi-Cucuzza, C., Tamborini, M., Pozzi, D., Barajon, I., Giorgino, T., Natalello, A., and Matteoli, M. (2016) Amyloid-β 1–24 C-terminal truncated fragment promotes amyloid-β 1–42 aggregate formation in the healthy brain. *Acta Neuropathol. Commun. 4*, 110.

53. Fonte, V., Dostal, V., Roberts, C. M., Gonzales, P., Lacor, P., Magrane, J., Dingwell, N., Fan, E. Y., Silverman, M. A., Stein, G. H., and Link, C. D. (2011) A glycine zipper motif mediates the formation of toxic β-amyloid oligomers in vitro and in vivo. *Mol. Neurodegener. 6*, 61.

54. Harmeier, A., Wozny, C., Rost, B. R., Munter, L.-M., Hua, H., Georgiev, O., Beyermann, M., Hildebrand, P. W., Weise, C., Schaffner, W., and Schmitz, D. (2009) Role of amyloid-β glycine 33 in oligomerization, toxicity, and neuronal plasticity. *J. Nanoneurosci. 29*, 7582–7590.

55. Stuyver, T., Danovich, D., and Shaik, S. (2019) Captodative Substitution Enhances the Diradical Character of Compounds, Reduces Aromaticity, and Controls Single-Molecule Conductivity Patterns: A Valence Bond Study. *J. Phys. Chem. A 123*, 7133–7141.

56. Viehe, H. G., Janousek, Z., Merenyi, R., and Stella, L. (1985) The captodative effect. *Acc. Chem. Res. 18*, 148–154.

57. Green, M. C., Stelzleni, S., and Francisco, J. S. (2013) Spectral Marker for Cα Damage in Beta Peptides. *J. Phys. Chem. A 117*, 550–565.

58. Davies, M. J. (2005) The oxidative environment and protein damage. *Biochim. Biophys. Acta, Proteins Proteomics 1703*, 93–109.

59. Song, Y., Li, P., Liu, L., Bortolini, C., and Dong, M. (2018) Nanostructural Differentiation and Toxicity of Amyloid-β25-35 Aggregates Ensue from Distinct Secondary Conformation. *Sci. Rep. 8*, 765.

60. Hughes, E., Burke, R. M., and Doig, A. J. (2000) Inhibition of Toxicity in the β-Amyloid Peptide Fragment β-(25–35) Using N-Methylated Derivatives A GENERAL STRATEGY TO PREVENT AMYLOID FORMATION. *J. Biol. Chem. 275*, 25109–25115.

61. Karplus, M., and McCammon, J. A. (2002) Molecular dynamics simulations of biomolecules. *Nat. Struct. Mol. Biol. 9*, 646.

62. Dror, R. O., Jensen, M. Ø., Borhani, D. W., and Shaw, D. E. (2010) Exploring atomic resolution physiology on a femtosecond to millisecond timescale using molecular dynamics simulations. *J. Gen. Physiol. 135*, 555–562.

63. Owen, M. C., Strodel, B., Csizmadia, I. G., and Viskolcz, B. (2016) Radical formation initiates solvent-dependent unfolding and β-sheet formation in a model helical peptide. *J. Phys. Chem. B 120*, 4878–4889.

64. Owen, M. C., Csizmadia, I. G., Viskolcz, B., and Strodel, B. (2017) Protein stability and unfolding following glycine radical formation. *Molecules 22*, 655.

65. Liao, Q., Owen, M. C., Bali, S., Barz, B., and Strodel, B. (2018) Aβ under stress: the effects of acidosis, Cu^{2+}-binding, and oxidation on amyloid β-peptide dimers. *Chem. Commun. (Cambridge, U. K.) 54*, 7766–7769.

66. Komáromi, I., Owen, M. C., Murphy, R. F., and Lovas, S. (2008) Development of glycyl radical parameters for the OPLS-AA/L force field. *J. Comput. Chem. 29*, 1999–2009.

67. Meli, M., and Colombo, G. (2013) A Hamiltonian replica exchange molecular dynamics (MD) method for the study of folding, based on the analysis of the stabilization determinants of proteins. *Int. J. Mol. Sci. 14*, 12157–12169.

68. Allen, W. J., Lemkul, J. A., and Bevan, D. R. (2009) GridMAT-MD: a grid-based membrane analysis tool for use with molecular dynamics. *J. Comput. Chem. 30*, 1952–1958.

69. Gapsys, V., de Groot, B. L., and Briones, R. (2013) Computational analysis of local membrane properties. *J. Comput.-Aided Mol. Des. 27*, 845–858.

70. Persson, F., Söderhjelm, P., and Halle, B. (2018) The geometry of protein hydration. *J. Chem. Phys. 148*, 215101.

71. Fox, S. J., Lakshminarayanan, R., Beuerman, R. W., Li, J., and Verma, C. S. (2018) Conformational Transitions of Melittin between Aqueous and Lipid Phases: Comparison of Simulations with Experiments. *J. Phys. Chem. B 122*, 8698–8705.

72. Matthes, D., and De Groot, B. L. (2009) Secondary structure propensities in peptide folding simulations: a systematic comparison of molecular mechanics interaction schemes. *Biophys. J. 97*, 599–608.

73. Mandal, P. K., and Pettegrew, J. W. (2004) Alzheimer's disease: NMR studies of asialo (GM1) and trisialo (GT1b) ganglioside interactions with Aβ (1-40) peptide in a membrane mimic environment. *Neurochem. Res. 29*, 447–453.

74. Rosenman, D. J., Connors, C. R., Chen, W., Wang, C., and García, A. E. (2013) Aβ monomers transiently sample oligomer and fibril-like configurations: Ensemble characterization using a combined MD/NMR approach. *J. Mol. Biol. 425*, 3338–3359.

75. L. Fawzi, N., Phillips, A. H., Ruscio, J. Z., Doucleff, M., Wemmer, D. E., and Head-

Gordon, T. (2008) Structure and dynamics of the Aβ21–30 peptide from the interplay of NMR experiments and molecular simulations. *J. Am. Chem. Soc. 130*, 6145–6158.

76. Carballo-Pacheco, M., and Strodel, B. (2017) Comparison of force fields for Alzheimer's Aβ42: A case study for intrinsically disordered proteins. *Protein Sci. 26*, 174–185.

77. Nasica-Labouze, J., Nguyen, P. H., Sterpone, F., Berthoumieu, O., Buchete, N.-V., Cote, S., De Simone, A., Doig, A. J., Faller, P., Garcia, A., and Laio, A. (2015) Amyloid β protein and Alzheimer's disease: When computer simulations complement experimental studies. *Chem. Rev. (Washington, DC, U. S.) 115*, 3518–3563.

78. Man, V. H., He, X., Derreumaux, P., Ji, B., Xie, X.-Q., Nguyen, P. H., and Wang, J. (2019) Effects of All-Atom Molecular Mechanics Force Fields on Amyloid Peptide Assembly: The Case of Aβ16–22 Dimer. *J. Chem. Theory Comput. 15*, 1440–1452.

79. Ding, H., Schauerte, J. A., Steel, D. G., and Gafni, A. (2012) β-amyloid (1–40) peptide interactions with supported phospholipid membranes: A single-molecule study. *Biophys. J. 103*, 1500–1509.

80. Korshavn, K. J., Satriano, C., Lin, Y., Zhang, R., Dulchavsky, M., Bhunia, A., Ivanova, M. I., Lee, Y.-H., La Rosa, C., Lim, M. H., and Ramamoorthy, A. (2017) Reduced lipid bilayer thickness regulates the aggregation and cytotoxicity of amyloid-β. *J. Biol. Chem. 292*, 4638–4650.

81. Qiang, W., Yau, W.-M., and Schulte, J. (2015) Fibrillation of β amyloid peptides in the presence of phospholipid bilayers and the consequent membrane disruption. *Biochim. Biophys. Acta, Biomembr. 1848*, 266–276.

82. Terzi, E., Hölzemann, G., and Seelig, J. (1995) Self-association of β-amyloid peptide (1–40) in solution and binding to lipid membranes. *J. Mol. Biol. 252*, 633–642.

83. Manna, M., and Mukhopadhyay, C. (2013) Binding, conformational transition and dimerization of amyloid-β peptide on GM1-containing ternary membrane: insights from molecular dynamics simulation. *PLoS One 8*, No. e71308.

84. Tachi, Y., Okamoto, Y., and Okumura, H. (2019) Conformational Change of Amyloid-β 40 in Association with Binding to GM1-Glycan Cluster. *Sci. Rep. 9*, 6853.

85. Vivekanandan, S., Brender, J. R., Lee, S. Y., and Ramamoorthy, A. (2011) A partially folded structure of amyloid-beta (1–40) in an aqueous environment. *Biochem. Biophys. Res. Commun. 411*, 312–316.

86. Ledeen, R. (1978) Ganglioside structures and distribution: are they localized at the nerve ending? *J. Supramol. Struct. 8*, 1–17.

87. Amaro, M., Šachl, R., Aydogan, G., Mikhalyov, I. I., Vácha, R., and Hof, M. (2016) GM1 Ganglioside Inhibits β-Amyloid Oligomerization Induced by Sphingomyelin. *Angew. Chem., Int. Ed. 55*, 9411–9415.

88. Ariga, T., McDonald, M. P., and Robert, K. Y. (2008) Thematic Review Series: Sphingolipids. Role of ganglioside metabolism in the pathogenesis of Alzheimer's disease–a review. *J. Lipid Res. 49*, 1157–1175.

89. Tomaselli, S., Esposito, V., Vangone, P., van Nuland, N. A., Bonvin, A. M., Guerrini, R., Tancredi, T., Temussi, P. A., and Picone, D. (2006) The α-to-β conformational transition of Alzheimer's Aβ-(1–42) peptide in aqueous media is reversible: A step by step conformational analysis suggests the location of β conformation seeding. *ChemBioChem 7*, 257–267.

90. Jorgensen, W. L., Chandrasekhar, J., Madura, J. D., Impey, R. W., and Klein, M. L. (1983) Comparison of simple potential functions for simulating liquid water. *J. Chem. Phys. 79*, 926–935.

91. Kaminski, G. A., Friesner, R. A., Tirado-Rives, J., and Jorgensen, W. L. (2001) Evaluation and reparametrization of the OPLS-AA force field for proteins via comparison with accurate quantum chemical calculations on peptides. *J. Phys. Chem. B 105*, 6474–6487.

92. Kulig, W., Pasenkiewicz-Gierula, M., and Róg, T. (2015) Topologies, structures and parameter files for lipid simulations in GROMACS with the OPLS-aa force field: DPPC, POPC, DOPC, PEPC, and cholesterol. *Data Brief 5*, 333–336.

93. Maciejewski, A., Pasenkiewicz-Gierula, M., Cramariuc, O., Vattulainen, I., and Rog, T. (2014) Refined OPLS all-atom force field for saturated phosphatidylcholine bilayers at full hydration. *J. Phys .Chem. B 118*, 4571–4581.

94. Hess, B., Kutzner, C., Van Der Spoel, D., and Lindahl, E. (2008) GROMACS 4: algorithms for highly efficient, load-balanced, and scalable molecular simulation. *J. Chem. Theory Comput. 4*, 435–447.

95. Zhang, J. (2015) The Hybrid Idea of (Energy Minimization) Optimization Methods Applied to Study Prion Protein Structures Focusing on the beta2-alpha2 Loop. *Biochem. Pharmacol. (Los Angeles, CA, U. S.) 4*, 2167–0501.

96. Müller, K., and Brown, L. D. (1979) Location of saddle points and minimum energy paths by a constrained simplex optimization procedure. *Theor. Chim. Acta 53*, 75–93.

97. Bussi, G., Donadio, D., and Parrinello, M. (2007) Canonical sampling through velocity rescaling. *J. Chem. Phys. 126*, 014101.

98. Parrinello, M., and Rahman, A. (1980) Crystal structure and pair potentials: A molecular-dynamics study. *Phys. Rev. Lett. 45*, 1196.

99. Parrinello, M., and Rahman, A. (1981) Polymorphic transitions in single crystals: A new molecular dynamics method. *J. Appl. Phys. (Melville, NY, U. S.) 52*, 7182–7190.

100. Parrinello, M., and Rahman, A. (1982) Strain fluctuations and elastic constants. *J. Chem. Phys 76*, 2662–2666.

101. Nosé, S. (1984) A unified formulation of the constant temperature molecular dynamics methods. *J. Chem. Phys. 81*, 511–519.

102. Nosé, S. (1986) An extension of the canonical ensemble molecular dynamics method. *Mol. Phys. 57*, 187–191.

103. NOSÉ, S. U. I. (2002) A molecular dynamics method for simulations in the canonical ensemble. *Molecular Physics 100*, 191–198.

104. Hoover, W. G. (1985) Canonical dynamics: Equilibrium phase-space distributions. *Phys. Rev. A 31*, 1695.

105. Darden, T., York, D., and Pedersen, L. (1993) Particle mesh Ewald: An N·log (N) method for Ewald sums in large systems. *J. Chem. Phys. 98*, 10089–10092.

106. Essmann, U., Perera, L., Berkowitz, M. L., Darden, T., Lee, H., and Pedersen, L. G. (1995) A smooth particle mesh Ewald method. *J. Chem. Phys. 103*, 8577–8593.

107. Hess, B., Bekker, H., Berendsen, H. J., and Fraaije, J. G. (1997) LINCS: a linear constraint solver for molecular simulations. *J. Comput. Chem. 18*, 1463–1472.

108. Bussi, G. (2014) Hamiltonian replica exchange in GROMACS: a flexible implementation. *Mol. Phys. 112*, 379–384.

109. Tribello, G. A., Bonomi, M., Branduardi, D., Camilloni, C., and Bussi, G. (2014) PLUMED 2: New feathers for an old bird. *Comput. Phys. Commun. 185*, 604–613.

110. M.J. Abraham, E. L. B. H., D. van der Spoel, and the GROMACS development team, GROMACS User Manual. version 2018.2, www.gromacs.org (2018).

111. Abraham, M. J., Murtola, T., Schulz, R., Páll, S., Smith, J. C., Hess, B., and Lindahl, E. (2015) GROMACS: High performance molecular simulations through multi-level parallelism from laptops to supercomputers. *SoftwareX 1*, 19–25.

112. Páll, S., Abraham, M. J., Kutzner, C., Hess, B., and Lindahl, E. Solving Software Challenges for Exascale. International Conference on Exascale Applications and Software, Stockholm, Sweden, April 2-3, 2014; Laure, S. M., Ed. ; Springer: Cham, 2015; pp 3–27.

113. Pronk, S., Páll, S., Schulz, R., Larsson, P., Bjelkmar, P., Apostolov, R., Shirts, M. R., Smith, J. C., Kasson, P. M., Van Der Spoel, D., and Hess, B. (2013) GROMACS 4.5: a high-throughput and highly parallel open source molecular simulation toolkit. *Bioinformatics 29*, 845–854.

114. Kabsch, W., and Sander, C. (1983) Dictionary of protein secondary structure: pattern recognition of hydrogen-bonded and geometrical features. *Biopolymers 22*, 2577–2637.

115. Daura, X., Gademann, K., Jaun, B., Seebach, D., Van Gunsteren, W. F., and Mark, A. E. (1999) Peptide folding: when simulation meets experiment. *Angew. Chem., Int. Ed. 38*, 236–240.

116. Humphrey, W., Dalke, A., and Schulten, K. (1996) VMD: visual molecular dynamics. *J. Mol. Graphics 14*, 33–38.

Graphical TOC Entry